ACS Catalysis

Research Article

pubs.acs.org/acscatalysis

The Influence of the Second and Outer Coordination Spheres on Rh(diphosphine)$_2$ CO_2 Hydrogenation Catalysts

J. Timothy Bays, Nilusha Priyadarshani, Matthew S. Jeletic, Elliot B. Hulley, Deanna L. Miller, John C. Linehan,* and Wendy J. Shaw*

Pacific Northwest National Laboratory, Richland, Washington 99354, United States

Supporting Information

ABSTRACT: A series of $[Rh(PCH_2X^RCH_2P)_2]^+$ complexes was prepared to investigate second and outer coordination sphere effects on CO_2 hydrogenation catalysis, where X is CH_2 (dppp) or X−R is N−CH_3, N−CH_2COOH (glycine), N−CH_2COOCH_3 (Gly-OMe), or N−CH_2C(O)N−CH(CH_3)-COOCH_3 (GlyAla-OMe). All of these complexes were active for CO_2 reduction to formate, with the N−CH_3 derivative offering an 8-fold enhancement over the dppp derivative, which is consistent with increased electron density around the metal. Despite the increase in rate with the addition of the pendant nitrogen, the addition of electron withdrawing amino acids and dipeptides to the amine resulted in complexes with reductions in rate of 1 to 2 orders of magnitude, most consistent with a change in pK_a of the pendant amine, resulting in lower activity. Collectively, the data suggest multiple contributions of the pendant amine in this catalytic system.

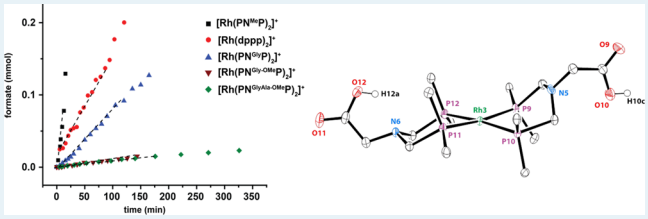

KEYWORDS: *CO_2 hydrogenation, amino acid catalysts, outer coordination sphere, homogeneous catalysis, in situ NMR*

INTRODUCTION

The carbon dioxide levels in the atmosphere are constantly increasing and research into mitigating and/or utilizing the carbon dioxide is underway.[1] Our interests are in using CO_2 as an energy conduit by which energy, preferably generated through renewable means, can be stored and released on demand.[2] In our current research, we seek to store energy by hydrogenating CO_2 to formic acid (as formate) or methanol.

We have previously demonstrated the use of a first row transition metal, cobalt(bis)diphosphine, catalyst system to hydrogenate CO_2 to formate with H_2 at ambient temperatures and pressure in the presence of a base.[3] The cobalt case demonstrated that through the use of known thermodynamic parameters, an efficient catalyst system can be designed. In the present study, our interest is directed away from the metal center, and toward the second and outer coordination spheres around the catalytic metal. We have demonstrated significant enhancements to catalytic activity for hydrogen production and oxidation catalysts, due to concentrating substrate, controlling the structure of the active site, and enhancing proton movement through the use of the second and outer coordination spheres of molecular catalysts.[4] Similar contributions may enhance catalysts for CO_2 hydrogenation and may offer insight into the mechanism. Here, we maintain the (bis)diphosphine first coordination sphere, to which we add a second coordination sphere containing an amine, and an outer coordination sphere bearing mono- and dipeptides. We utilize rhodium, as rhodium(diphosphine)$_2$ complexes are well-known CO_2 hydrogenation catalysts,[5] providing a well-understood core for incorporating an outer coordination sphere. The introduction of these functional groups is facilitated by the three-atom backbone separating the phosphines. This backbone contains an easily functionalized group such as an amine (second coordination sphere), e.g. a PN^RP ligand (PNP: $R'_2P-CH_2-N^R-CH_2-PR'_2$), to which amino acids can be attached.

Tuning the second and outer coordination spheres of CO_2 hydrogenation catalysts for rate enhancement is only starting to be investigated. A recent report by Fujita et al. describes the role of a pendant base in the second sphere for efficient CO_2 hydrogenation, where the amine group is proposed to deprotonate the dihydride and to hydrogen bond to CO_2.[6] Work by Schmeier et al. demonstrates the use of a hydrogen bond donor in the second coordination sphere to facilitate CO_2 insertion.[7] Herein, we describe the catalytic activity of $Rh(PX^RP)_2$ complexes, where X is a carbon, a substituted nitrogen, or the amine of an amino acid. The results show positive catalytic activity due to the presence of the N−CH_3 instead of the CH_2 group, while additions to the amine beyond the methyl group result in losses in activity. These results are explained by electrostatic modulations at the active site and changes in pK_a of the pendant amine due to the modifications in the second and outer coordination spheres.

RESULTS

Synthesis of Diphosphine (PN^RP) Ligands and Metal Complexes. Five $[Rh(PX^RP)_2]^+$ complexes were prepared (Figure 1, Scheme 1), where X^R = CH_2 (dppp; 1,3-(bisdiphenylphosphino)propane), N−CH_3, N−CH_2COOH

Received: June 27, 2014
Revised: September 2, 2014
Published: September 3, 2014

 © 2014 American Chemical Society dx.doi.org/10.1021/cs5009199 | ACS Catal. 2014, 4, 3663−3670

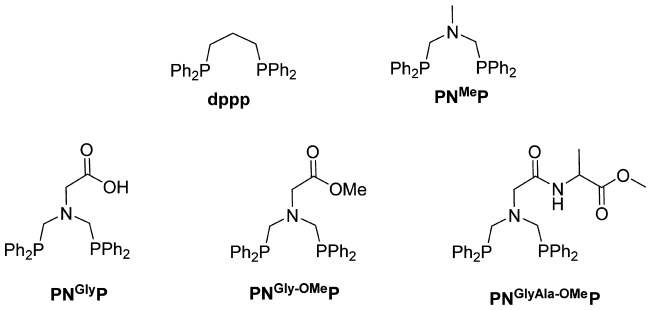

Figure 1. Diphosphine ligands and abbreviations used in these studies.

Scheme 1. Synthesis of PN^{R}P Diphosphine Ligands Containing Amino Acids

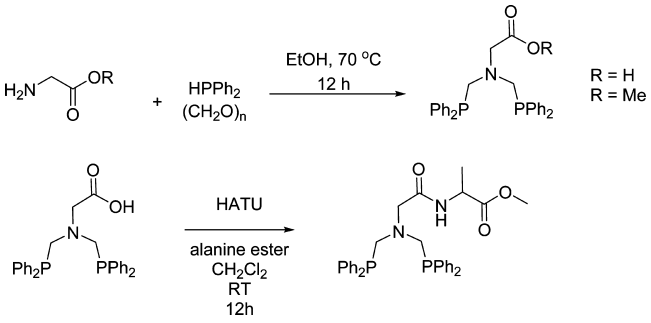

(glycine, Gly), N−CH_2COOCH_3 (glycine methyl ester, Gly-OMe), and N−$CH_2C(O)$N−$CH(CH_3)COOCH_3$ (glycine-alanine methyl ester, GlyAla-OMe). The synthesis of PN^{Me}P was previously reported,[8] and dppp was used as purchased. The amine of glycine or glycine methyl ester was directly incorporated into the **PN^{R}P** backbone in a one pot reaction of the amino acid, diphenyl phosphine ($HPPh_2$), and paraformaldehyde in ethanol to result in PN^{Gly}P and PN$^{Gly\text{-}OMe}$P, analogous to the previously reported method.[8] The dipeptide containing ligand, PN$^{GlyAla\text{-}OMe}$P, was prepared by coupling alanine to the COOH group of PN^{Gly}P, using standard FMOC chemistry protocols.[9] Ligands were purified by multiple washes and separation from ethanol. All three ligands were characterized by ^{1}H and ^{31}P{^{1}H} NMR spectroscopy and metalated without further characterization. PN$^{GlyAla\text{-}OMe}$P was further characterized using 2D ^{1}H-TOCSY NMR spectroscopy to confirm that amino acid coupling was complete. In all cases, characterization was consistent with the proposed structures and with previous ligands of this type.[8]

The metal complexes were prepared by adding two equivalents of the ligand in tetrahydrofuran to one equivalent of $[Rh(COD)_2]OTf$ at room temperature (Scheme 2). All metal complexes were prepared and isolated as yellow powders in good yields (~80%) and characterized by elemental analysis, mass spectral data, and ^{1}H and ^{31}P{^{1}H} NMR spectroscopy. The resulting metal complexes exhibit a characteristic doublet in the ^{31}P{^{1}H} NMR spectra corresponding to the Rh−P coupling ($^1J_{Rh-P}$ = 130−131 Hz; Table 1 and Figure S1). The ^{31}P{^{1}H} chemical shift for $[Rh(dppp)_2]^+$ is shifted downfield of the others (8.7 ppm vs ~7.0 ppm), suggesting decreased electron density at the phosphorus for this complex, while the electron density for the amine-containing complexes remained essentially constant, vida infra. Crystal structures were obtained for $[Rh(dppp)_2]OTf$, $[Rh(PN^{Me}P)_2]OTf$, and $[Rh(PN^{Gly}P)_2]OTf$ (Figure 2). Selected bond distances and angles are given in Table 2 and Table S1. The bite angles for the two bidentate ligands for $[Rh(dppp)_2]^+$ are both 86.24°, for $[Rh(PN^{Me}P)_2]^+$ are 88.02°, and for $[Rh(PN^{Gly}P)_2]^+$ are 86.58° and 85.40°, consistent with a nearly square planar geometry and consistent with values found for similar Rh complexes.[10] Two unique molecules crystallized for $[Rh(PN^{Me}P)_2]^+$ and four unique molecules crystallized for $[Rh(PN^{Gly}P)_2]^+$. The additional distances are reported in Tables S2 and S3.

Catalytic Hydrogenation of Carbon Dioxide. Each of the complexes studied was active for CO_2 hydrogenation at room temperature under 40 atm of 1:1 CO_2/H_2 in the presence of Verkade's base (2,8,9-triisopropyl-2,5,8,9-tetraaza-1-phosphabicyclo[3.3.3]undecane; Figure 3) in d_8-THF. Catalytic studies were performed in a high-pressure PEEK cell setup previously described (Table 3).[3,11] Rates (turnover frequency, TOF) of reaction decrease in activity in the following order: $[Rh(PN^{Me}P)_2]^+ > [Rh(dppp)_2]^+ \simeq [Rh(PN^{Gly}P)_2]^+ > [Rh(PN^{Gly\text{-}OMe}P)_2]^+ \simeq [Rh(PN^{GlyAla\text{-}OMe}P)_2]^+$. TOFs were measured by monitoring the increase in the integrated intensity of the formate ^{1}H NMR resonance at 8.7 ppm (Figure 4), relative to the increasing areas of two resonances corresponding to protonated Verkade's base at 6.15 and 5.15 ppm in the ^{1}H NMR (Figure S2). Due to the deprotonation of the $[H_2Rh(diphosphine)_2]^+$ complexes by Verkade's base, the rate can also be determined by the growing ^{31}P{^{1}H} NMR resonance of protonated Verkade's base, providing a second method of measuring the TOF. The two methods agreed within 10% of one another. The turnover number (TON) was limited by the amount of base available to deprotonate the dihydride and stabilize the formate produced, and except as noted, the reactions consumed the available Verkade's base. ^{1}H and ^{31}P{^{1}H} NMR spectra obtained during catalysis showed only the presence of monohydride, suggesting that CO_2 activation is the slow step in the process.

Thermodynamic Studies. To provide mechanistic insight into the catalytic observations, stoichiometric studies to observe the products of H_2 addition and deprotonation were performed in THF for each $[Rh(PX^RP)_2]^+$ complex, and the resulting products were characterized by ^{1}H and ^{31}P{^{1}H} NMR spectroscopy. A series of spectra for $[Rh(PN^{Gly}P)_2]^+$ is shown in Figure 5, representative of all complexes, which show similar spectral changes. In each case dihydrides were observed upon the addition of 1 atm of H_2, based on two apparent doublets of triplets in the ^{31}P{^{1}H} NMR spectra, and the appearance of a doublet in the ^{1}H NMR (Figure 5 and Table 1). The observed broad ^{31}P{^{1}H} NMR splitting patterns are common for an AA′XX′M spin system of a *cis*-$[H_2Rh(PX^RP)_2]^+$ complex,[12]

Scheme 2. Synthesis of Rh(bis)diphosphine Metal Complexes

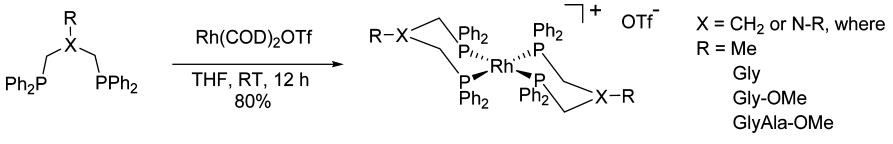

dx.doi.org/10.1021/cs5009199 | ACS Catal. 2014, 4, 3663−3670

Table 1. $^{31}P\{^1H\}$ and ^1H NMR Assignments for Each Metal Complex, Dihydride ($[H_2Rh(PX^RP)_2]^+$), and Hydride ($HRh(PX^RP)_2$)

complex	$^{31}P\{^1H\}$ NMR (ppm)	$^1J_{RhP}$ (Hz)	$^2J_{PP}$ (Hz)	^1H NMR hydride peak (ppm)	$^2J_{PH}$ (Hz)	$^1J_{RhH}$ (Hz)
$[Rh(dppp)_2]^+$	8.7	131				
$[Rh(PN^{Me}P)_2]^+$	6.9	131				
$[Rh(PN^{Gly}P)_2]^+$	6.9	130				
$[Rh(PN^{Gly\text{-}OMe}P)_2]^+$	7.2	131				
$[Rh(PN^{GlyAla\text{-}OMe}P)_2]^+$	7.4	130				
$[H_2Rh(dppp)_2]^+$	20.3, 7.7	96, 84[a]	30, *b*	−8.55	142	13
$[H_2Rh(PN^{Me}P)_2]^+$	14.9, −0.5	99, 86[a]	30, *b*	−8.7	140	*c*
$[H_2Rh(PN^{Gly}P)_2]^+$	15.1, −3.5	108,[a] 90[b]	*b*	−8.9	140	*c*
$[H_2Rh(PN^{Gly\text{-}OMe}P)_2]^+$	14.3, −4.5	95,[a] 80[b]	*b*	−8.9	140	*c*
$[H_2Rh(PN^{GlyAla\text{-}OMe}P)_2]^+$	14.7, −3.6	*b*	*b*	−8.9	*b*	*c*
$HRh(dppp)_2$	18.5	142	*c*	−10.3	21[a]	8[a]
$HRh(PN^{Me}P)_2$	16.7	142	*c*	−11.0	18[a]	10[a]
$HRh(PN^{Gly}P)_2$	16.6	142	*c*	−11.4	*b*	*b*
$HRh(PN^{Gly\text{-}OMe}P)_2$	15.2	142	*c*	−10.8	*c*	*c*
$HRh(PN^{GlyAla\text{-}OMe}P)_2$	15.5	142	*c*	−10.9	*c*	*c*

[a]Estimated from NMR spectra, not taking into account second order effects. [b]Poorly resolved. [c]Not observed.

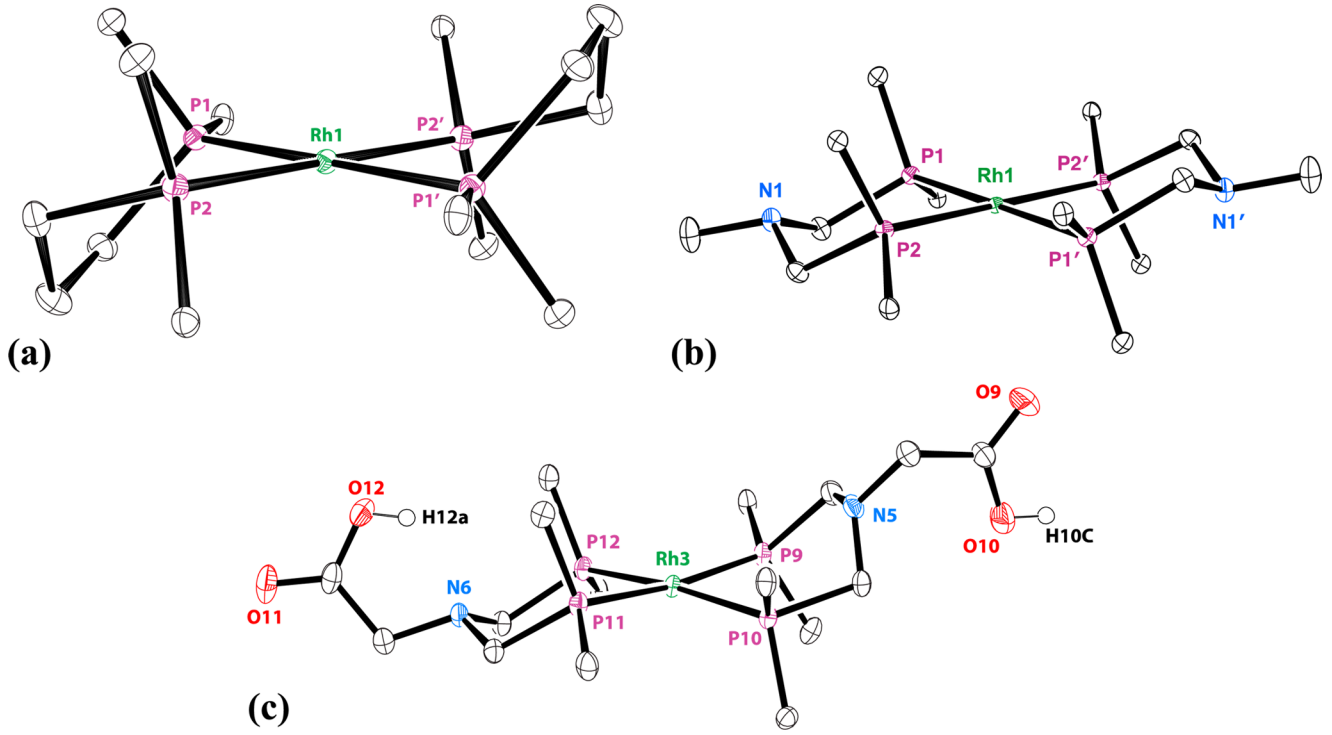

Figure 2. Solid-state structures of (a) $[Rh(dppp)_2]^+$, (b) $[Rh(PN^{Me}P)_2]^+$, and (c) $[Rh(PN^{Gly}P)_2]^+$ depicted with 50% probability ellipsoids. Noncritical hydrogen atoms, phenyl ring carbons (except the *ipso* carbons), anions, and solvent molecules have been omitted for clarity.

shown in Figure 5b. The doublet in the ^1H NMR is consistent with an octahedral Rh-dihydride complex, where the large coupling has been previously assigned to the $^2J_{PH}$ coupling, confirmed with NMR studies (Figure S3).[13] Significantly more of the dihydride species was observed for the $[Rh(dppp)_2]^+$ complex, evidence that H_2 addition is more favorable for this complex than the others. The calculated ΔG_{H_2} values for H_2 addition to the complexes are presented in Table 4 and increase in the following order: $[Rh(dppp)_2]^+ < [Rh(PN^{Gly\text{-}OMe}P)_2]^+ < [Rh(PN^{Me}P)_2]^+ \simeq [Rh(PN^{Gly}P)_2]^+ < [Rh(PN^{GlyAla\text{-}OMe}P)_2]^+$. Consistent with the parent complexes, the $^{31}P\{^1H\}$ resonances for the $[H_2Rh(dppp)_2]^+$ complex (20.3 and 7.7 ppm) are significantly downfield of the resonances for the complexes with pendant amines (~15 and −3 ppm). This observation is consistent with maintained lower electron density at the phosphorus atoms in the $[H_2Rh(dppp)_2]^+$ complexes. Conversion between starting material and the dihydride complex was shown to be reversible by the reappearance of starting material when the hydrogen was removed under a vacuum. In all cases, adding Verkade's base resulted in the complete conversion of all species to the monohydride, with similar chemical shifts observed in both $^{31}P\{^1H\}$ and ^1H NMR spectra, consistent with a square pyramidal structure with the monohydride having four equivalent phosphines, as shown by a doublet in the $^{31}P\{^1H\}$ NMR and an AX_4M coupling pattern in the ^1H NMR (Figure 5c). Once again, the $^{31}P\{^1H\}$ resonance for $[Rh(dppp)_2]^+$ is downfield of the $^{31}P\{^1H\}$

dx.doi.org/10.1021/cs5009199 | ACS Catal. 2014, 4, 3663−3670

Table 2. Selected Bond Distances (Å) and Angles (deg) for $[Rh(dppp)_2]^+$, $[Rh(PN^{Me}P)_2]^+$, and $[Rh(PN^{Gly}P)_2]^+$

$[Rh(dppp)_2]^{+a}$		$[Rh(PN^{Me}P)_2]^{+a}$		$[Rh(PN^{Gly}P)_2]^+$	
Rh1−P1	2.3285(3) Å	Rh1−P1	2.3314(11) Å	Rh3−P9	2.3086(8) Å
Rh1−P2	2.3151(3) Å	Rh1−P2	2.3473(13) Å	Rh3−P10	2.3243(8) Å
Rh1−P1′	2.3285(3) Å	Rh1−P1′	2.3314(11) Å	Rh3−P11	2.3301(8) Å
Rh1−P2′	2.3151(3) Å	Rh1−P2′	2.3473(13) Å	Rh3−P12	2.3041(8) Å
P1−Rh1−P2	86.237(12)°	P1−Rh1−P2	88.02(4)°	P9−Rh3−P10	85.40(3)°
P2−Rh1−P1′	93.762(12)°	P2−Rh1−P1′	91.98(4)°	P10−Rh3−P11	94.63(3)°
P1′−Rh1−P2′	86.237(12)°	P1′−Rh1−P2′	88.02(4)°	P11−Rh3−P12	86.58(3)°
P2′−Rh1−P1	93.762(12)°	P2′−Rh1−P1	91.98(4)°	P12−Rh3−P9	94.15(3)°
P1−Rh1−P1′	180°	P1−Rh1−P1′	180°	P9−Rh3−P11	172.67(3)°
P2−Rh1−P2′	180°	P2−Rh1−P2′	180°	P10−Rh3−P12	174.06(3)°
dihedral[b]	0°	dihedral[b]	0°	dihedral[b]	9.74(1)°

[a]Atoms labeled with primes are symmetry generated based on the crystallographic space groups (see SI for more information). [b]The dihedral is defined as the angle between the two planes formed by P1−Rh1−P2 and P1′−Rh1−P2′ or P10−Rh3−P9 and P11−Rh3−P12.

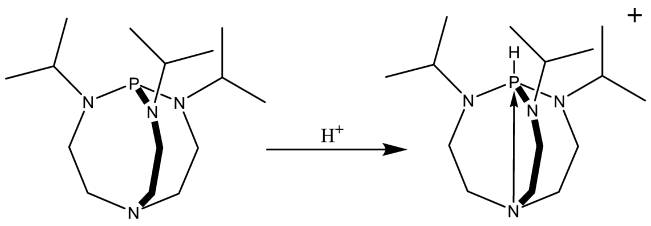

Figure 3. Reaction of Verkade's base, 2,8,9-triisopropyl-2,5,8,9-tetraaza-1-phosphabicyclo[3.3.3]undecane, with acid.

Table 3. Rates of Hydrogenation of CO_2 for Each Metal Complex in THF[a]

catalyst[b]	$[M^+]$ (mM)	[Vkd][d] (mM)	TOF (h^{-1})	TON
$[Rh(dppp)_2]^+$	1.1	420	150 ± 50	370
$[Rh(PN^{Me}P)_2]^+$	1.5	390	920 ± 20	280
$[Rh(PN^{Gly}P)_2]^+$	1.1	410	120 ± 10	370
$[Rh(PN^{Gly\text{-}OMe}P)_2]^+$	1.5	330	11 ± 4	220[c]
$[Rh(PN^{GlyAla\text{-}OMe}P)_2]^+$	1.0	380	12 ± 7	370[c]

[a]Catalytic conditions: 350-400 μL d_8-THF, 1:1 CO_2/H_2, 600 psi (40 atm) at 21 °C. No formate was detected in the absence of catalyst. [b]All Rh catalysts were triflate (OTf^-) salts. All reactions went to completion, consuming the Verkade's base, except as noted. [c]60−70% conversion based upon time constraints. [d]Vkd = 2,8,9-triisopropyl-2,5,8,9-tetraaza-1-phosphabicyclo[3,3,3] undecane, Verkade's base (Figure 3).

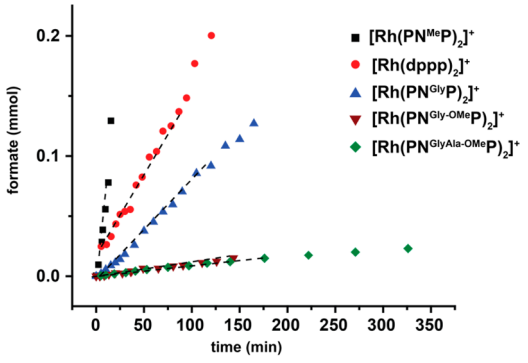

Figure 4. Formate formed vs time for each of the metal complexes. Black squares, $[Rh(PN^{Me}P)_2]^+$; red circles, $[Rh(dppp)_2]^+$; blue triangles, $[Rh(PN^{Gly}P)_2]^+$; maroon inverted triangles, $[Rh(PN^{Gly\text{-}OMe}P)_2]^+$; and green diamonds, $[Rh(PN^{GlyAla\text{-}OMe}P)_2]^+$. Regions fit to obtain kinetic rates are shown by dashed lines.

resonance for the other complexes. Formate was produced when the H_2 atmosphere was replaced with 1 atm of CO_2, with some, but not all, of the monohydride species returning to the starting material, Figure 5d. Addition of a 1:1 CO_2/H_2 atmosphere to the reaction mixture caused the slow growth of the formate peak.

DISCUSSION

Including second and outer coordination spheres into CO_2 hydrogenation catalysts has the potential to enhance catalytic activity by orders of magnitude, as has been observed for other catalysts, such as those for hydrogen production and oxidation.[4,14] In this work, we focus on including a pendant amine in the second coordination sphere and amino acid functionalities in the outer coordination sphere. Each of these groups could influence one of the three steps in the proposed catalytic cycle, (1) H_2 addition, (2) deprotonation of the dihydride, and (3) hydride transfer/formate loss, as shown in Figure 6.

Effect of the Pendant Amine (Second Coordination Sphere). The rate of formate production increases by approximately an order of magnitude by substituting $N-CH_3$ for the central methylene unit of dppp (Table 3), $[Rh(PN^{Me}P)_2]^+$ and $[Rh(dppp)_2]^+$, respectively. In the absence of Verkade's base, deprotonation of the dihydride to form the monohydride is not observed, suggesting that the pendant amine in $[Rh(PN^{Me}P)_2]^+$ is not acting as an unassisted base. However, the $^{31}P\{^1H\}$ NMR spectroscopic data suggest that the electron density at the phosphorus atoms increases significantly upon the introduction of the amine functionalities, based on the upfield shift in the $^{31}P\{^1H\}$ resonances (Table 1) from those observed for $[Rh(dppp)_2]^+$. Increased electron density at the rhodium would be expected to enhance the hydride donor ability, facilitating the formation of formate, step 3 in the proposed catalytic cycle (Figure 6). Changes in electron density at the phosphorus atoms may result from either inductive effects or strain-induced changes in the bonding of the bidentate ligands to the rhodium. The similarity in the crystal structures of $[Rh(dppp)_2]^+$ and $[Rh(PN^{Me}P)_2]^+$ suggest strain-induced changes are not responsible for the observed differences in rate.

In addition to the altered electrostatics at the metal site, there are other possible roles that the pendant amine could play. Recently, the stabilization of H_2 or CO_2 near the active site by the pendant amine has been proposed in other work;[6a,b,7] however, this is not observed in our system. Indeed, the lack of

dx.doi.org/10.1021/cs5009199 | ACS Catal. 2014, 4, 3663−3670

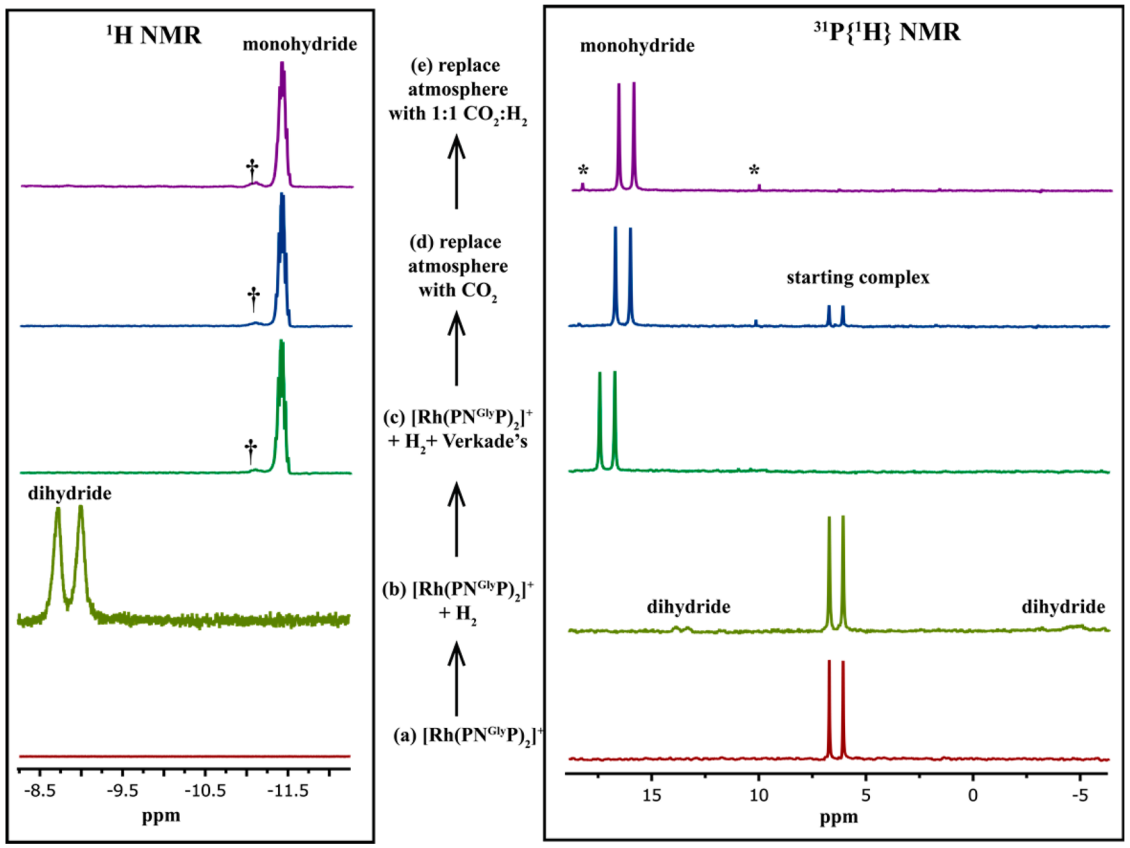

Figure 5. Select regions of the ^{1}H (left) and ^{31}P{^{1}H} NMR (right) spectra for $(PN^{Gly}P)_2RhOTf$ as reagents were added to a J. Young tube to gain insight into the catalytic cycle. Chemical shift differences of the monohydride observed upon adding CO_2 in the ^{31}P{^{1}H} NMR spectra are due to decreased polarity or density of the solvent upon dissolution of CO_2. †A minor hydride peak. *Decomposition products of Verkade's base.[3]

Table 4. Thermodynamic Parameters for the Dihydride Complexes, $[H_2Rh(PX^RP)_2]^+$[a]

complex	K_{eq}[b] (atm^{-1})	ΔG_{H_2} (kcal/mol)
$[H_2Rh(dppp)_2]^+$	6.7	−1.1
$[H_2Rh(PN^{Me}P)_2]^+$	0.27	+0.77
$[H_2Rh(PN^{Gly}P)_2]^+$	0.30	+0.71
$[H_2Rh(PN^{Gly\text{-}OMe}P)_2]^+$	0.49	+0.41
$[H_2Rh(PN^{GlyAla\text{-}OMe}P)_2]^+$	0.09[c]	+1.4

[a]All reactions were carried out in a J. Young NMR tube at 1 atm H_2 pressure. [b]The units for K_{eq} result from the use of conditions that are nonstandard state (i.e., $[H_2]$ is not 1M). [c]Only limited hydrogen addition was observed (<5%).

correlation between the ΔG_{H_2} and the catalytic rates is a strong indication that hydrogen addition (step 1) is not the rate limiting step for catalysis, and consequently, the effect of the pendant amine must alter a different step, such as CO_2 activation or formate formation (step 3). A recent report by Himeda et al. indicated that thermodynamically unfavorable CO_2 insertion into the metal-H bond at room temperature can be facilitated by hydrogen bonding interactions with a second coordination sphere base, and it is possible that the pendant amine is playing such a role here.[6a,b,7] To provide further insight into the role of the pendant amine, the complexes containing an amine with amino acids or dipeptides are considered.

Effect of Amino Acids and Dipeptides (Outer Coordination Sphere). The incorporation of an amino acid, an amino ester, or a dipeptide into the bidentate PN^RP ligand reduces the catalytic rate by 1, 2, and 2 orders of magnitude, respectively (Table 3), compared to that of $[Rh(PN^{Me}P)_2]^+$. Yet very little change is observed in the ^{31}P{^{1}H} NMR resonances among all of the $[Rh(PN^RP)_2]^+$ complexes, suggesting that the electron density at the metal has not changed appreciably with the addition of these electron withdrawing groups. The observed reductions in rate are clearly not due to a steric effect resulting from the larger amino

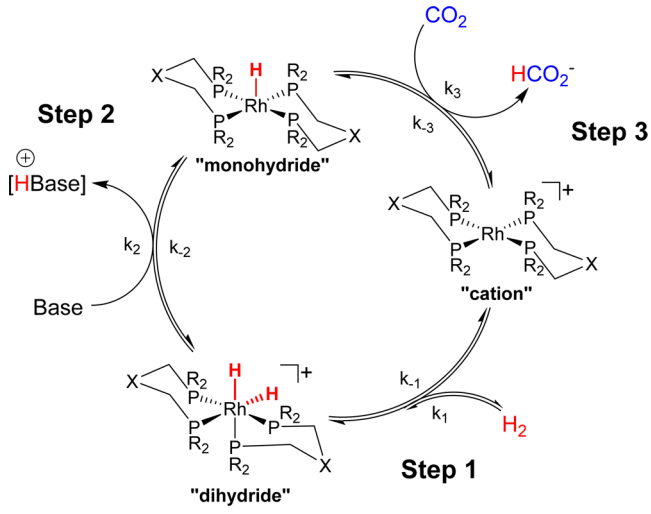

Figure 6. Proposed catalytic mechanism for the hydrogenation of CO_2.[3]

dx.doi.org/10.1021/cs5009199 | ACS Catal. 2014, 4, 3663−3670

acid and dipeptide groups, since both the $[Rh(PN^{Gly\text{-}OMe}P)_2]^+$ and $[Rh(PN^{GlyAla\text{-}OMe}P)_2]^+$ have similar rates, but significantly different steric properties, while the rates for $[Rh(PN^{Gly}P)_2]^+$ and $[Rh(PN^{Gly\text{-}OMe}P)_2]^+$ are very different, despite having similar steric properties. The small deviation from an ideal planar geometry observed for $[Rh(PN^{Gly}P)_2]^+$ relative to $[Rh(PN^{Me}P)_2]^+$ and $[Rh(dppp)_2]^+$ might be expected for all amino-acid-containing complexes, suggesting that differences in rate of formate production might arise from distortions introduced by the amino acids in the bidentate ligands. Other contributions to the observed differences in rate may result from the influence of functional groups on the pendant amine, or through interaction of the outer coordination sphere with the rhodium or with the hydrides in the first coordination sphere during deprotonation (step 2) or CO_2 activation (step 3) in the proposed catalytic cycle (Figure 6).

Studies of $Ni(P_2^RN_2^{R'})_2$ and $Ni(P_2^RN^{R'})_2$ systems have shown that N-substituents strongly affect the pK_a of the pendant amine.[14b,15] This was specifically demonstrated for complexes containing electron withdrawing C(O)O−R groups, the presence of which resulted in a lower pK_a of the pendant amine.[15b] It is expected that the COOH and C(O)O−R groups appended to the $[Rh(PN^RP)_2]^+$ complexes would also reduce the pK_a of the pendant amine. Collectively, these data suggest that the lower pK_a of the pendant amine, due to the electron withdrawing groups, hinders catalysis, as compared to the higher rate observed for the electron donating methyl substituent. These data further imply that in addition to the pendant amine increasing electron density at the metal, the pK_a of the pendant amine plays a critical role in the catalytic cycle. Possible explanations consistent with a dependence on pendant amine pK_a would be a role in assisting Verkade's base in dihydride deprotonation (step 2), or in another scenario, that the pendant amine hydrogen bonds to the Rh−H, weakening the hydride bond to facilitate the formation of formate. The former effect would ideally be tested with a weaker base; however, due to the slow nature of these complexes, testing a weaker base would result in catalysis too slow to measure using in situ techniques. The latter effect has been predicted computationally for the $Ni(P^R_2N^{R'}_2H)_2$ systems where additional functional groups or steric effects weaken the ($Ni^0\cdots$H−N), lowering the barrier to deprotonation, and a similar mechanism may be operating here.[15b,16] The same logic could be used to explain the enhanced rate of $[Rh(PN^{Gly}P)_2]^+$ compared to $[Rh(PN^{Gly\text{-}OMe}P)_2]^+$ and $[Rh(PN^{GlyAla\text{-}OMe}P)_2]^+$. When $[Rh(PN^{Gly}P)_2]^+$ is in the carboxylate form, the form observed during the highly basic catalytic conditions, the amine becomes slightly more electron donating compared to the amines of $[Rh(PN^{Gly\text{-}OMe}P)_2]^+$ and $[Rh(PN^{GlyAla\text{-}OMe}P)_2]^+$, increasing the p$K_a$ of the pendant amine, thereby increasing the ability of the pendant amine to interact with a first coordination sphere hydride. Alternately, the carboxylate may be directly interacting with a first coordination sphere hydride, similarly weakening the Rh···H interaction. In either mechanism, the contribution is not as favorable as that of $[Rh(PN^{Me}P)_2]^+$. While the precise mechanism is not yet well-defined, it is clear from the collective data that the second and outer coordination spheres play important roles in determining overall catalytic activity. Developing a more detailed mechanistic model of this enzyme-inspired control will be the focus of future studies.

SUMMARY

In order to expand the understanding of the second and outer coordination spheres on the catalytic rates of CO_2 hydrogenation, pendant amines, single amino acids, or dipeptides were incorporated into $[Rh(PN^RP)_2]^+$ metal complexes. These amino acid functionalized $[Rh(PN^RP)_2]^+$ complexes are active for CO_2 reduction with significant sensitivity to the presence of the amine and the amine functional group. The contribution of the amine is two-fold: to increase the electron density at the metal and to provide a basic functional group sufficiently close to the metal to participate in some fashion during catalysis. Our data further suggest that lowering the pK_a of this group reduces catalytic activity. Additional studies are necessary to more definitively establish the role of the pendant amine, as well as the influence of a larger outer coordination sphere, in the catalytic cycle.

EXPERIMENTAL SECTION

General Methods. All chemical reactions were performed under an inert atmosphere on a Schlenk line or in a glovebox unless otherwise noted. The diphosphine ligand, dppp, and Verkade's base were purchased from Sigma-Aldrich and used without further purification. d_8-THF was dried over a sodium−potassium amalgam. Other organic solvents were dried and degassed by a standard solvent purification system. UHP (ultra high purity) CO_2 and H_2 were purchased from Oxarc. The polyetherether ketone (PEEK) high-pressure NMR tubes were designed and built at Pacific Northwest National Laboratory.[11] ^1H and $^{13}C\{^1H\}$ NMR spectra were recorded on Varian Inova 500 MHz or VNMRS 300 MHz NMR spectrometers. ^1H and $^{13}C\{^1H\}$ NMR chemical shifts are referenced to $CDCl_3$, CD_3CN, or d_8-THF. $^{31}P\{^1H\}$ NMR spectra were obtained on a Varian Inova 500 spectrometer. Chemical shifts are reported referenced to external 85% H_3PO_4 (0 ppm). Under catalytic conditions, $^{31}P\{^1H\}$ NMR chemical shifts in THF were referenced to protonated Verkade's base at −11.9 ppm in the absence of CO_2, or −12.9 ppm in the presence of CO_2, which were separately referenced to 85% H_3PO_4 (0 ppm) from the atmospheric pressure experiments. Mass analysis was performed using a 15T Fourier transform ion cyclotron resonance mass spectrometer (FTICR-MS) (Bruker SolariX, Billerica, MA) outfitted with a standard electrospray ionization (ESI) interface. For characterization of crystal structures, a suitable crystal was selected, immersed in paratone-N oil, placed on a nylon loop, and mounted under a cold stream of N_2. The crystal was kept at 100(2) K during data collection. A Bruker KAPPA APEX II CCD diffractometer with 0.71073 Å Mo Kα radiation was used for diffraction studies. Data collection and cell refinement were performed using Bruker APEX2 software. Data reductions and absorption corrections were performed using Bruker's SAINT and SADABS programs.[17] A direct method structure solution and a Least Squares minimization refinement were completed using SHELXS-97 and SHELXL-97,[18] respectively, using the OLEX2 software package[19] as a front end.

General Procedure for Catalysis. In a glovebox, ∼40 mg of Verkade's base was dissolved in 200 μL of d_8-THF, then added to the PEEK tube followed by 50 μL of the catalyst at the desired dilution. The volume was then made to a total volume of between 330 and 390 μL with d_8-THF to result in final catalyst concentrations of 1.1−1.5 mM and final Verkade's base concentrations of 330−420 mM. The PEEK tube was then

dx.doi.org/10.1021/cs5009199 | ACS Catal. 2014, 4, 3663−3670

valved off and transferred to the ISCO pump apparatus. A pseudo freeze−pump−thaw method was used to eliminate N_2 from the tube.[3] Then the 1:1 CO_2/H_2 gas mix was delivered at a constant pressure of 40 atm using an ISCO syringe pump. The PEEK tube was placed on a vortex mixer to allow for gas mixing when NMR spectra were not being recorded. Quantitative $^{31}P\{^1H\}$ and proton NMR spectra were collected between 2 and 5 min apart.

The amount of conversion at each time point was determined in the following way. The ratios of the areas of the Verkade's base and protonated Verkade's base obtained from the quantitative $^{31}P\{^1H\}$ spectrum yield the amount of protonated Verkade's base. The comparison of the areas of the formate and the protonated Verkade's base in the quantitative proton NMR spectrum then yields the amount of formate produced. Turnover frequencies (TOFs) were calculated from the slope of the linear portion of kinetic plots, such as those displayed in Figure 4. The TOFs quoted in Table 3 were the average of three experiments run under identical conditions. $^{31}P\{^1H\}$ NMR spectra were collected at time zero and after catalysis was complete, and periodically during the reaction.

General Procedure for the Synthesis of PN^RP Ligand. To a 50 mL Schlenk flask equipped with a magnetic stir bar was added diphenylphosphine (0.72 g, 0.30 mmol) and paraformaldehyde (0.132 g, 0.344 mmol) in 30 mL of ethanol. The resulting cloudy solution was stirred for 2 h at room temperature. Then, the amino acid derivative was added and heated to 70 °C for 12 h under N_2. Upon completion of the reaction, ethanol was evaporated under reduced pressure to obtain a white crystalline solid in good yield.

$PN^{Gly}P$. The reaction was carried out at 1 mmol scale, and the product was isolated as a white solid in 90% yield. ^1H NMR (500 MHz, $CDCl_3$): δ 3.64 (s, 2H, N-CH_2-COOH), 3.67 (s, 2H, P-CH_2-N), 3.68 (s, 2H, P-CH_2-N), 7.27−7.45 (m, 20H, P-Ph-*H*). $^{13}C\{^1H\}$ NMR (125 MHz, $CDCl_3$): δ 29.85 (N-CH_2-COOH), 59.01 (P-CH_2-N), 59.11 (P-CH_2-N), 128.82 (d, $^3J_{PC}$ = 7.1 Hz, *m*-C-Ph), 129.35 (s, *p*-C-Ph), 133.07 (d, $^2J_{PC}$ = 18.9 Hz, *o*-C-Ph), 133.32 (d, $^1J_{PC}$ = 11.6 Hz, P-C-Ph), 171.40 (N−CH_2−COOH). $^{31}P\{^1H\}$ NMR (202 MHz, $CDCl_3$): δ −26.8.

$PN^{Gly\text{-}OMe}P$. The reaction was performed at 1 mmol scale to afford the product as a white solid in 85% yield. ^1H NMR (500 MHz, CD_3CN): δ 3.59 (s, 3H, −COOCH_3), 3.72 (s, 2H, P-CH_2-N), 3.73 (s, 2H, P-CH_2-N), 3.78 (s, 2H), 7.27−7.45 (m, 20H, P-Ph-*H*). $^{31}P\{^1H\}$ NMR (202 MHz, CD_3CN): δ −26.8.

Synthesis of $PN^{GlyAla\text{-}OMe}P$. To a solution of dichloromethane (5 mL) containing $PN^{Gly}P$ was added HATU (1-[bis-(dimethylamino)methylene]-1H-1,2,3-triazolo[4,5-*b*]-pyridinium 3-oxid hexafluorophosphate) (96 mg, 0.47 mmol) and diisopropylethylamine (DIPEA) (115 mg, 0.89 mmol) and stirred for 15 min. Then, alanine methyl ester was added to the reaction vial and stirred for 12 h at room temperature. After 12 h, the organic phase was washed with water (5 mL × 3), and the organic layer was dried with anhydrous magnesium sulfate. The organic layer was evaporated under reduced pressure to yield an off-white solid in 60% yield. ^1H NMR (500 MHz, CD_3CN): δ 0.88 (d, *J* = 7.3 Hz, 3H, N-αCH-CH_3), 3.51 (s, 2H, N-CH_2-CONH), 3.60 (m, 7H, COOCH_3 and PCH_2N), 4.13 (m, 1H, N-αC*H*-CH$_3$), 6.70 (d, $J_{NH\text{-}\alpha CH}$ = 6.8 Hz, CON*H*), 7.21−7.54 (m, 20H, P-*Ph*-*H*). $^{31}P\{^1H\}$ NMR (202 MHz, CD_3CN): δ −26.7.

General Procedure for the Synthesis of Rh Metal Complex. To a solution of the PN^RP ligand (1 mmol) in THF, 0.5 mmol of $Rh(COD)_2OTf$ was added dropwise and stirred 6−12 h to obtain a clear yellow colored solution. The THF solution was concentrated to 1 mL under reduced pressure and was then added dropwise to a flask containing 10 mL of diethyl ether to precipitate the product as a yellow suspension. The product was filtered through a medium frit and dried to afford the Rh catalyst in good yield. Crystals were grown from THF via solvent evaporation to yield yellow or orange block shaped crystals.

$[Rh(dppp)_2]OTf$. The reaction was carried out following the above procedure to isolate the product in 92% yield. ^1H NMR (500 MHz, $CDCl_3$): δ 1.88 (s, 4H, P-CH_2-CH_2-), 2.27 (s, 8H, P-CH_2-CH_2-), 7.14−7.28 (m, 40H, P-Ph-*H*). $^{13}C\{^1H\}$ NMR (125 MHz, $CDCl_3$): δ 18.8 (P-CH_2-CH_2), 29.0 (m, P-CH_2-CH_2), 128.9 (*m*-C-Ph), 130.8 (*p*-C-Ph), 132.2(*o*-C-*Ph*), 133.6 (m, P-C-Ph). $^{31}P\{^1H\}$ NMR (202 MHz, $CDCl_3$): δ 8.7 (d, J_{RhP} = 131 Hz). ESI MS: Observed (M^+- *OTf*) at *m*/*z*: 1077.16 and calculated (M^+- *OTf*) as 1077.18. Elem anal. calcd. for C, 61.23; H, 5.05. Found: C, 61.80; H, 5.98.

$[Rh(PN^{Me}P)_2]^+$. The reaction was carried out as outlined above, and the product was isolated as a yellow solid in 62% yield. ^1H NMR (500 MHz, $CDCl_3$): δ 2.33 (s, 8H, P-CH_2-N), 3.16 (s, 6H, N-CH_3), 7.34−7.09 (m, 40H, P-Ph-*H*). $^{13}C\{^1H\}$ NMR (125 MHz, $CDCl_3$): δ 50.43 (N-CH_3), 60.21 (m, P-CH_2-N), 128.38 (*m*-C-Ph),, 130.48 (*p*-C-Ph), 132.62(m, P-C-Ph), 130.13 (*o*-C-Ph). $^{31}P\{^1H\}$ NMR (202 MHz, $CDCl_3$): δ 7.19 (d, J_{RhP} = 130 Hz). ESI MS: Observed (M^+-OTf) at *m*/*z*: 957.23 and calculated (M^+-OTf) as 957.84. Elem anal. calcd. for C, 59.57; H, 5.09; N, 2.53. Found: C, 59.28; H, 5.03; N, 2.46.

$[Rh[(PN^{Gly}P)_2]^+$. The reaction was carried out as outlined above, and the product was isolated as a yellow solid in 78% yield. ^1H NMR (500 MHz, $CDCl_3$): δ 3.62 (s, 4H, P-CH_2-N), 3.64 (s, 4H, P-CH_2-N), 3.65 (s, 4H, N-CH_2-COOH), 7.23−7.40 (M, 40H, P-Ph-*H*), 10.99 (s, 1H, N-CH_2-COO*H*). $^{13}C\{^1H\}$ NMR (125 MHz, $CDCl_3$): δ 30.11 (N-CH_2-COOH), 60.11 (m, P-CH_2-N),128.32 (*m*-C-Ph), 129.57 (*p*-C-Ph), 133.08 (*o*-C-Ph), 134.33 (bs, P-C-Ph), 171.01 (-COOH). $^{31}P\{^1H\}$ NMR (202 MHz, $CDCl_3$): δ 7.00 (d, J_{RhP} = 130 Hz). ESI MS: Observed (M^+) at *m*/*z*: 1194.16 and calculated (M^+) as 1196.18. Elem anal. calcd. for C, 59.57; H, 5.09; N, 2.53. Found: C, 59.28; H, 5.03; N, 2.46.

$[Rh(PN^{Gly\text{-}OMe}P)_2]^+$. The reaction was carried out at 1 mmol scale to obtain a yellow solid in 69% yield. ^1H NMR (500 MHz, CD_3CN): δ 3.34 (s, 4H, N-CH_2-COOCH_3), 3.71 (s, 6H, COOCH_3), 3.79 (s, 8H, P-CH_2-N), 7.11−7.60 (m, 40H, P-Ph-*H*). $^{13}C\{^1H\}$ NMR (125 MHz, CD_3CN): δ 50.85 (N-CH_2-COOCH_3), 56.28 (N-CH_2-COOCH_3), 60.17 (P-CH_2-N), 128.08 (*m*-C-Ph), 130.01 (*p*-C-Ph), 132.63 (bs, P-C-Ph), 133.21 (*o*-C-Ph), 170.79 (-COOCH_3). $^{31}P\{^1H\}$ NMR (202 MHz, CD_3CN): δ 7.07 (d, J_{RhP} = 131 Hz). ESI MS: Observed (M^+- *OTf*) at *m*/*z*: 1073.25 and calculated (M^+- *OTf*) as 1073.24. Elem anal. calcd. for C, 57.94; H, 4.78; N, 2.29. Found: C, 56.69; H, 5.09; N, 2.26. (Elemental analysis characterization for amino acid containing complexes have typically not passed, despite confirmation of indicated complex based on all other characterization methods.)

$[Rh(PN^{GlyAla\text{-}OMe}P)_2]^+$. Following the general procedure above, the reaction was carried out at 1 mmol scale to obtain a yellow solid in 62% yield. ^1H NMR (500 MHz, CD_3CN): δ 1.24 (bs, 6H, NH-αCH-CH_3), 3.32 (s, 4H, N-CH_2-COONH-), 3.61−4.06 (m, 14H, P-CH_2-N and -COOCH_3), 4.30 (m, 2H, NH-αC*H*-CH3), 6.92 (s, 2H, COON*H*), 7.59−8.31 (m, 40H, P-Ph-*H*). $^{13}C\{^1H\}$ NMR (125 MHz, CD_3CN): δ 22.51 (αCH-CH_3), 53.52 (N-CH_2-COONH), 53.57 (αCH-CH_3), 57.60

dx.doi.org/10.1021/cs5009199 | *ACS Catal.* 2014, 4, 3663−3670

($COOCH_3$), 62.80 (m, P-CH_2-N), 133.56 (*m*-C-Ph), 135.72 (*p*-C-Ph), 137.88 (bs, P-C-Ph), 139.14 (*o*-C-Ph), 174.30 (-COONH), 178.61 (-$COOCH_3$). $^{31}P\{^1H\}$ NMR (202 MHz, CD_3CN): δ 7.7 (d, J_{RhP} = 130 Hz). ESI MS: Observed (M^+-*OTf*) at *m*/*z* 1215.39 and calculated (M^+- *OTf*) as 1215.31. Elem anal. calcd. for C, 57.19; H, 5.02; N, 4.10; Found: C, 52.54; H, 5.42; N, 4.28. (Elemental analysis characterization for amino acid containing complexes have typically not passed, despite confirmation of indicated complex based on all other characterization methods.)

■ ASSOCIATED CONTENT

Supporting Information

^{31}P NMR spectra of the starting Rh metal complexes. Representative ^{31}P and ^1H NMR of $[Rh(PN^{Gly}P)_2]^+$. ^1H and $^1H\{^{31}P\}$ spectra of $[Rh(dppp)_2]^+$ and $[H_2Rh(dppp)_2]^+$. Crystallographic data. This material is available free of charge via the Internet at http://pubs.acs.org/.

■ AUTHOR INFORMATION

Corresponding Authors

*P.O. Box 999 MS: K2-57 Richland, WA 99354. Phone: 509-375-5922. E-mail: wendy.shaw@pnnl.gov.

*P.O. Box 999 MS: K2-57 Richland, WA 99354. Phone: 509-375-3983. E-mail: john.linehan@pnnl.gov.

Notes

The authors declare no competing financial interest.

■ ACKNOWLEDGMENTS

The authors would like to thank Dr. Aaron Appel for helpful discussions. This work was supported by the U.S. Department of Energy, Office of Basic Energy Sciences, Division of Chemical Sciences, Geosciences & Biosciences. Pacific Northwest National Laboratory (PNNL) is a multiprogram national laboratory operated for the DOE by Battelle. A portion of this research was performed using EMSL, a national scientific user facility sponsored by the Department of Energy's Office of Biological and Environmental Research and located at Pacific Northwest National Laboratory.

■ REFERENCES

(1) (a) Peters, M.; Kohler, B.; Kuckshinrichs, W.; Leitner, W.; Markewitz, P.; Muller, T. E. *ChemSusChem* **2011**, *4*, 1216−1240. (b) Darensbourg, D. J. *Inorg. Chem.* **2010**, *49*, 10765−10780. (c) Appel, A. M.; Bercaw, J. E.; Bocarsly, A. B.; Dobbek, H.; DuBois, D. L.; Dupuis, M.; Ferry, J. G.; Fujita, E.; Hille, R.; Kenis, P. J. A.; Kerfeld, C. A.; Morris, R. H.; Peden, C. H. F.; Portis, A. R.; Ragsdale, S. W.; Rauchfuss, T. B.; Reek, J. N. H.; Seefeldt, L. C.; Thauer, R. K.; Waldrop, G. L. *Chem. Rev.* **2013**, *113*, 6621−6658. (d) Jessop, P. G.; Ikariya, T.; Noyori, R. *Chem. Rev.* **1995**, *95*, 259−272. (e) Jessop, P. G.; Joo, F.; Tai, C. C. *Coord. Chem. Rev.* **2004**, *248*, 2425−2442. (f) Federsel, C.; Jackstell, R.; Beller, M. *Angew. Chem., Int. Ed.* **2010**, *49*, 6254−6257. (g) Cokoja, M.; Bruckmeier, C.; Rieger, B.; Herrmann, W. A.; Kuhn, F. E. *Angew. Chem., Int. Ed.* **2011**, *50*, 8510−8537. (h) Wang, W.; Wang, S.; Ma, X.; Gong, J. *Chem. Soc. Rev.* **2011**, *40*, 3703−3727.

(2) (a) Savéant, J.-M. *Chem. Rev.* **2008**, *108*, 2348. (b) Benson, E. E.; Kubiak, C. P.; Sathrum, A. J.; Smieja, J. M. *Chem. Soc. Rev.* **2009**, *38*, 89. (c) Cook, T. R.; Dogutan, D. K.; Reece, S. Y.; Surendranath, Y.; Teets, T. S.; Nocera, D. G. *Chem. Rev.* **2010**, *110*, 6474. (d) Thoi, V. S.; Sun, Y.; Long, J. R.; Chang, C. J. *Chem. Soc. Rev.* **2013**, *42*, 2388.

(3) Jeletic, M. S.; Mock, M. T.; Appel, A. M.; Linehan, J. C. *J. Am. Chem. Soc.* **2013**, *135*, 11533−11536.

(4) (a) Dutta, A.; Lense, S.; Hou, J.; Engelhard, M.; Roberts, J. A. S.; Shaw, W. J. *J. Am. Chem. Soc.* **2013**, *135*, 18490−18496. (b) Dutta, A.; Roberts, J. A. S.; Shaw, W. J. *Angew. Chem., Int. Ed.* **2014**, *53*, 6487−6491. (c) Jain, A.; Lense, S.; Linehan, J. C.; Raugei, S.; Cho, H.; DuBois, D. L.; Shaw, W. J. *Inorg. Chem.* **2011**, *50*, 4073−4085. (d) Jain, A.; Reback, M. L.; Lindstrom, M. L.; Thogerson, C. E.; Helm, M. L.; Appel, A. M.; Shaw, W. J. *Inorg. Chem.* **2012**, *51*, 6592−6602. (e) Reback, M. L.; Buchko, G. W.; Kier, B. L.; Ginovska-Pangovska, B.; Xiong, Y.; Lense, S.; Hou, J.; Roberts, J. A. S.; Sorensen, C. M.; Raugei, S.; Squier, T. C.; Shaw, W. J. *Chem.—Eur. J.* **2014**, 20. (f) Reback, M. L.; Ginovska-Pangovska, B.; Ho, M.-H.; Jain, A.; Squier, T. C.; Raugei, S.; Roberts, J. A. S.; Shaw, W. J. *Chem.—Eur. J.* **2013**, *19*, 1928−1941.

(5) (a) Jessop, P. G.; Joo, F.; Tai, C.-C. *Coord. Chem. Rev.* **2004**, *248*, 2425−2442. (b) Leitner, W. *Angew. Chem. Int. Ed.* **1995**, *34*, 2207−2221.

(6) (a) Fujita, E.; Muckerman, J. T.; Himeda, Y. *BBA: Bioenergetics* **2013**, *1827*, 1031−1038. (b) Wang, W.-H.; Hull, J. F.; Muckerman, J. T.; Fujita, E.; Himeda, Y. *Energy Environ. Sci.* **2012**, *5*, 7923−7926. (c) Zhang, Z. Y.; Xu, Z. J.; Yang, Z.; Liu, Y. T.; Wang, J. A.; Shao, Q.; Li, S. J.; Lu, Y. X.; Zhu, W. L. *J. Phys. Chem. B* **2013**, *117*, 4827−4835.

(7) Schmeier, T. J.; Dobereiner, G. E.; Crabtree, R. H.; Hazari, N. *J. Am. Chem. Soc.* **2011**, *133*, 9274−9277.

(8) Weiss, C. J.; Groves, A. N.; Mock, M. T.; Dougherty, W. G.; Kassel, W. S.; Helm, M. L.; DuBois, D. L.; Bullock, R. M. *Dalton Trans.* **2012**, *41*, 4517−4529.

(9) (a) Carpino, L. A.; Han, G. Y. *J. Org. Chem.* **1972**, *37*, 3404−3409. (b) El-Faham, A.; Albericio, F. *Chem. Rev.* **2011**, *111*, 6557.

(10) Fornika, R. S. C.; Gorls, H.; Kessler, M.; Kruger, C.; Leitner, W. *Can. J. Chem.* **2001**, *79*, 642−648.

(11) Yonker, C. R.; Linehan, J. C. *Prog. Nucl. Magn. Reson. Spectrosc.* **2005**, *47*, 95−109.

(12) DuBois, D. L.; Blake, D. M.; Miedaner, A.; Curtis, C. J.; DuBois, M. R.; Franz, J. A.; Linehan, J. C. *Organometallics* **2006**, *25*, 4414−4419.

(13) (a) Koch, A.; Bargon, J. *Inorg. Chem.* **2001**, *40*, 533−539. (b) Gridnev, I. D.; Higashi, N.; Imamoto, T. *Organometallics* **2001**, *20*, 4542−4553.

(14) (a) Rakowski DuBois, M.; DuBois, D. L. *Chem. Soc. Rev.* **2009**, *38*, 62−72. (b) Shaw, W. J.; Helm, M. L.; DuBois, D. L. *Biochim. Biophys. Acta: Bioenergetics* **2013**, *1827*, 1123−1139.

(15) (a) Kilgore, U. J.; Roberts, J. A. S.; Pool, D. H.; Appel, A. M.; Stewart, M. P.; Rakowski DuBois, M.; Dougherty, W. G.; Kassel, W. S.; Bullock, R. M.; DuBois, D. L. *J. Am. Chem. Soc.* **2011**, *133*, 5861−5872. (b) Lense, S.; Ho, M. H.; Chen, S. T.; Jain, A.; Raugei, S.; Linehan, J. C.; Roberts, J. A. S.; Appel, A. M.; Shaw, W. *Organometallics* **2012**, *31*, 6719−6731. (c) Stewart, M. P.; Ho, M. H.; Wiese, S.; Lindstrom, M. L.; Thogerson, C. E.; Raugei, S.; Bullock, R. M.; Helm, M. L. *J. Am. Chem. Soc.* **2013**, *135*, 6033−6046.

(16) Lense, S.; Dutta, A.; Roberts, J. A. S.; Shaw, W. J. *Chem. Commun.* **2014**, *50*, 792−795.

(17) (a) *SAINT*; Bruker AXS Inc: Madison,WI, 2007. (b) *SADABS*; Bruker ASX Inc.: Madison, WI, 2007.

(18) Sheldrick, G. *Acta Crystallogr. A* **2008**, *64*, 112−122.

(19) Dolomanov, O. V.; Bourhis, L. J.; Gildea, R. J.; Howard, J. A. K.; Puschmann, H. *J. Appl. Crystallogr.* **2009**, *42*, 339−341.